Soft Matter

PAPER

View Article Online
View Journal | View Issue

Cite this: *Soft Matter*, 2017, 13, 2808

Tailoring single chain polymer nanoparticle thermo-mechanical behavior by cross-link density†

Suwon Bae,[a] Or Galant,[b] Charles E. Diesendruck[b] and Meredith N. Silberstein*[a]

Received 21st February 2017,
Accepted 20th March 2017

DOI: 10.1039/c7sm00360a

rsc.li/soft-matter-journal

Single chain polymer nanoparticles (SCPNs) are formed from intrachain cross-linking of a single polymer chain, making SCPN distinct from other polymer nanoparticles for which the shape is predefined before polymerization. The degree of cross-linking in large part determines the internal architecture of the SCPNs and therefore their mechanical and thermomechanical properties. Here, we use molecular dynamics (MD) simulations to study thermomechanical behavior of individual SCPNs with different underlying structures by varying the ratio of cross-linking and the degree of polymerization. We characterize the particles in terms of shape, structure, glass transition temperature, mobility, and stress response to compressive loading. The results indicate that the constituent monomers of SCPNs become less mobile as the degree of cross-linking is increased corresponding to lower diffusivity and higher stress at a given temperature.

1 Introduction

Internal architecture is a powerful way of controlling the response of both nanoscale and bulk polymers. For amorphous glassy polymers small amounts of cross-linking may reduce the yield stress and enhance ductility,[1,2] while large degrees of cross-linking increase strength, decrease toughness, and increase the glass transition temperature.[3–6] Polymer microparticles also show an increase in strength with significant increases in degree of cross-linking.[7] Elastomers typically show an increase in stiffness and an increase followed by decrease in tensile strength with increasing degree of cross-linking.[8–10] Polymer properties have also been manipulated through branched and dendritic structures.[11–14] In this manuscript we explore the mechanics of single chain polymer nanoparticles (SCPNs) as individual units with interest in both their own mechanics and their potential as an architecture for tailoring bulk polymers.

SCPNs are formed from intra-chain cross-linking of a single chain polymer.[15] In contrast to classic polymer nanoparticles, which are prepared in one step by microemulsion polymerization, SCPN internal structures can be tightly controlled through linear chain functionalization. Recently, SCPN synthesis techniques have been growing more sophisticated in terms of available monomer chemistries, tailoring options, and batch size.[16–23] For example, cross-links can be covalent or non-covalent, be located at random or specific locations on the chain, and occur among just two or among multiple locations simultaneously.[18–21] The structure of SCPNs is controlled by solvent quality as well as polymer chain composition.[23] While extensive work has gone into experimentally characterizing the size, structure, and chemistry of SCPNs,[24–26] little is known about the mechanical and thermomechanical properties of individual SCPNs. One hint into these properties is from Hosono *et al.* who conducted forced unfolding of SCPNs and observed consecutive peaks in force-extension curves from bond rupture events whose sequence and magnitude depended on the internal cross-link structure.[25]

Molecular dynamics (MD) is a common approach for studying the thermomechanical behavior of polymers.[27–33] It is advantageous over experiments for rapidly exploring dependencies on architectural choices and determining the underlying cause of a macroscopically observable property. For instance the potential energy in a specific bond angle can be trivially tracked throughout a deformation process. Despite the high strain rate inherent to the computational limits of an MD simulation, good agreement has been found with quasi-static mechanical tests.[27,34,35] For polymers, relatively low fidelity/low cost force fields (*e.g.* DREIDING, CHARMM, GROMACS, consistent valence force field, polymer consistent force field)[36–39] can be used to predict the stress–strain response and glass transition temperature. The compressive response of nanoparticles has previously been simulated through flat plate compression.[40–42] In these simulations the nanoparticles are placed between two flat plates, repulsive force

[a] *Sibley School of Mechanical and Aerospace Engineering, Cornell University, NY14850, USA. E-mail: ms2682@cornell.edu; Tel: +607 255 5063*
[b] *Schulich Faculty of Chemistry and Russell-Berrie Nanotechnology Institute, Technion – Israel Institute of Technology, Haifa, Israel*

† Electronic supplementary information (ESI) available: Radius of SCPNs, radius of gyration of SCPNs, radial density distribution of methylenes beads, cooling rate dependence of volume change, stress response of SCPNs, and energy decomposition as a function of degree of cross-linking. See DOI: 10.1039/c7sm00360a

is imposed between the plates and atoms within the particle, and the plates are moved towards each other at a constant velocity while force on the plates and particle configuration are monitored. This method was validated to give results that fall within the upper and low bounds given by elastic–plastic theory and Hertzian contact respectively.[40] MD has also previously been used to investigate SCPN, but these papers focused on the morphology as a function of cross-link locational selectivity[43] and presence of solvent.[44]

The goal of this study is to understand the effects of cross-linking ratio and degree of polymerization (DP) on the thermo-mechanical behavior of individual SCPNs through molecular dynamics simulations. We built MD models of polyethylene (PE)-like polymers as representative SCPN of three different DP and three different cross-linking ratios. Collapsed linear chains (no cross-linking) were also studied for reference. PE is chosen as a simple representative polymer since it has a structure that is readily course grained and all the common polymer interactions. The prepared SCPN were then analyzed in terms of initial particle structure, glass transition temperature, diffusivity, and compression response. All MD simulations were performed using the large-scale atomic/molecular massively parallel simulator (LAMMPS).[45]

2 Methods

2.1 MD model

A coarse-grained model was adopted to represent the PE chain that forms the SCPN. Each methylene group is treated as a single neutral bead. The interaction between beads were captured by a modified DREIDING potential. This course grained representation of PE with a DREIDING potential enables us to explore all the typical elements of a polymer interaction with reasonable computational cost. The total potential energy of a system is expressed as the sum of the bonded energy and non-bonded energy.

$$E_{\text{total}} = E_{\text{bonded}} + E_{\text{non-bonded}} \quad (1)$$

The bonded energy is comprised of the bond stretching, bond angle bending and torsional dihedral energies. The non-bonded energy is described only by the Lennard-Jones interaction.

$$E_{\text{bonded}} = E_{\text{bond}} + E_{\text{angle}} + E_{\text{dihedral}} \quad (2)$$

$$E_{\text{non-bonded}} = E_{\text{LJ}} \quad (3)$$

$$E_{\text{bond}} = \frac{1}{2}k_{\text{b}}(r - r_0)^2 \quad (4)$$

$$E_{\text{angle}} = \frac{1}{2}k_{\text{a}}(\theta - \theta_0)^2 \quad (5)$$

$$E_{\text{dihedral}} = \sum_{n=1}^{5} A_n \cos^{n-1}(\phi) \quad (6)$$

$$E_{\text{LJ}} = 4\varepsilon\left[\left(\frac{\sigma}{r}\right)^{12} - \left(\frac{\sigma}{r}\right)^{6}\right] \quad (7)$$

where k_{b}, k_{a} and A_n are force constants for bond stretching, bond angle bending and torsional dihedral terms respectively; r is the bond length of each bond and r_0 is the equilibrium bond length; θ is the angle between two bonds and θ_0 is the equilibrium angle; ϕ is the dihedral angle between planes made by two adjacent angles; ε is the depth of the Lennard-Jones potential wall, σ is the distance at which the inter-bead potential is zero, and r is the distance between two beads. The values for these parameters were adopted from a force field used in predicting macroscopic properties of amorphous PE.[35] A new cross-link was modeled as a bond that contributes to the total potential energy by eqn (4). The new angles and dihedrals introduced by new cross-links were set to take the same form as eqn (5) and (6) respectively.

Each SCPN was derived from a linear PE chain. A globular structure was generated by annealing the linear PE chain in vacuum from a perfectly planar all-*trans* zig–zag conformation. The annealing consisted of holding temperature at 500 K for 1 ns, cooling from 500 K to 300 K over 0.8 ns, and then maintaining at 300 K for another 6 ns under *NVT* dynamics with a Nosé-Hoover thermostat to control the temperature. This cooling rate of 0.25 K ps^{-1} was selected based on convergence of the volume *versus* temperature behavior at different rates following the work conducted by Fukui *et al.*, (see ESI† Fig. S4).[46] To avoid rotation of the chain, the total angular momentum was set to zero. The velocity-Verlet time stepping scheme was adopted.

The linear chain was converted into a cross-linkable chain with a particular target cross-linking ratio by assigning functionalized cross-link sites along the chain and then repeatedly cross-linking (Fig. 1). To carry out cross-linking at 500 K, the activated linear chain was subjected to the elevation of temperature from 300 K to 500 K over 0.8 ns and then equilibrated at 500 K for another 1 ns. Cross-linking at 500 K, a temperature at which there is significant thermal motion, allows the functionalized sites to "see" and possibly bond with a broad range of other beads so that the cross-linking is not limited to initially adjacent functionalized sites. The collapsed configuration of the linear precursor promotes cross-linking over a broad range of contour

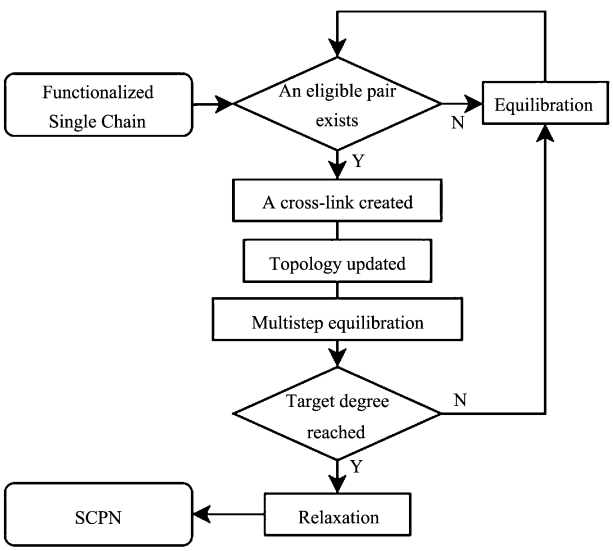

Fig. 1 Flowchart of cross-linking process.

lengths, which is similar to SCPN synthesis within a poor solvent.[44] The cross-linking process consisted of creation of one chemical bond and a subsequent multi-step equilibration. A distance only criteria was used to define eligible cross-linking pairs following the findings of Tam *et al.*, that neglecting bending and dihedral angles when establishing cross-links provides reasonable cross-linked polymer structures.[47] The upper limit of capture radius for cross-linking was set equal to the non-bonded interaction cutoff (10.5 Å). Every functionalized and not yet cross-linked site was investigated for its candidacy as a site to form a cross-link by calculating the distance to all other available sites and comparing it to a capture radius. Among eligible pairs a single pair was randomly chosen as the new cross-link location. If no eligible pairs were found the SCPN was equilibrated for an additional 0.1 ns before repeating the cross-link check. Once a cross-link was created, the topological data was updated with a new bond, new angles and new dihedrals. The updated MD model was then relaxed by a multi-step equilibration with a time step of 0.5 fs (Table 1).[48] Since it is likely that the initial bond length of the new cross-link is much larger than the bond equilibrium length the bond stiffness and the bond equilibrium length are gradually increased and decreased respectively to the actual value to prevent unrealistically high bond energies. The cross-linking process was repeated until the degree of cross-linking was within 0.5% from the target degree, *e.g.* the cross-linking process for 10% cross-link SCPN stopped once the degree reached higher than 9.5%. This was taken as a synthetically realistic range for a batch of particles. The system was cooled down from 500 K to 300 K at 0.25 K ps^{-1} and maintained at 300 K for another 6 ns. This algorithm was used to build cross-linked SCPNs 500, 1000, and 2000 monomers long with 5%, 10%, and 15% degree of cross-linking. For particles at 150 K the system was cooled from 300 K to 150 K at 0.25 K ps^{-1} and maintained at 150 K for another 6 ns.

2.2 Compression

The prepared SCPNs and collapsed linear chains were mechanically tested under flat plate compression as shown in Fig. 2. To apply compressive loading to SCPN, two flat plates were introduced above and below the particle. A repulsive potential was imposed between the plate and the beads that compose the SCPN as follows:

$$E(r) = K(r - R)^3 \quad (8)$$

Table 1 Force constants for a bond (a new cross-link) and the other bonds during multistep relaxation (r_0* is the bond equilibrium length and k_b* is the force constant of the regular bond)

		A cross-link		The other bonds	
Step	t (ps)	r_0	k_b	r_0	k_b
1	100	$r_0^* + (4/4)(d - r_0^*)$	$1/5 \times k_0^*$	r_0^*	k_0^*
2	100	$r_0^* + (3/4)(d - r_0^*)$	$2/5 \times k_0^*$		
3	100	$r_0^* + (2/4)(d - r_0^*)$	$3/5 \times k_0^*$		
4	100	$r_0^* + (1/4)(d - r_0^*)$	$4/5 \times k_0^*$		
5	100	$r_0^* + (0/4)(d - r_0^*)$	$5/5 \times k_0^*$		

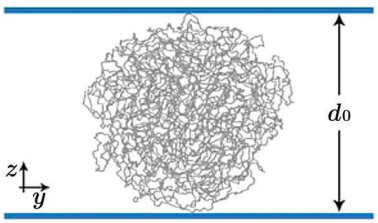

Fig. 2 Schematic of flat plate compression setup for molecular dynamics simulations.

where K is the force constant and $r - R$ is the normal distance in the compressive direction from the plate to a bead. The force constant was set to be 10 kcal (mole $Å^3)^{-1}$. Every bead that approaches the plate experiences a repulsive force with the magnitude of $3K(r - R)^2$ from the plate in the opposite direction along the compressive axis. Both plates were displaced towards each other at a constant speed corresponding to strain rate of 10^8 1 s^{-1}. The temperature was kept at either 300 K or 150 K during compression, as controlled by a Nosé–Hoover thermostat. The velocity-Verlet time stepping scheme was utilized with the velocities and positions of the beads were updated by time integration under *NVT* dynamics. Before the plates started moving and exerting a force on the beads, the total potential energy of the particle was minimized.

The force applied to the particle was obtained by measuring the force exerted on the plate. The net force was converted to stress, which is defined as the force divided by the initial cross-sectional area of the particle. For calculating stress, the cross-sectional area is defined as the mean ellipse that encompasses the projection of beads onto the x–y plane. The stress response was visualized *versus* strain, which is defined as the displacement of the plate divided by the initial plate to plate distance, d_0. Energy components were observed as a function of strain.

2.3 Particle analysis

The structures were analyzed in terms of shape, methylene radial distribution density, glass transition temperature, potential energy and methylene mobility. The shape was characterized by mean radius with standard deviation over time and spatial deviation. The mean radius was calculated by taking the geometric mean value of semi-principal axes.

The radial density was calculated with the center of mass of the SCPN located at the origin. Based on given lower and upper bounds of radius and the number of bins, spherical shell shaped bins were created (the innermost bin is a sphere) and the number of methylene beads falling within each bin and the corresponding mass were calculated. The mass was then divided by the volume of the bin and converted to density.

The glass transition temperature (T_g) of an individual SCPN was calculated by monitoring the evolution of total energy with temperature, *i.e.* the calculated T_g is an internal T_g of a single particle and does not include the interaction between several SCPNs. Each particle was cooled from 500 K to 10 K at a cooling rate of 0.25 K ps^{-1}. Total energies were recorded at 100 discrete temperatures with an interval of about 5 K. Two straight lines

were fitted to 100 pairs of total energy *versus* temperature. The intersection of these two fitted lines was taken as the T_g of that SCPN. The calorimetric method was chosen because of its common use in the MD literature and the relatively clear transition.[46,49–51] Implementation details, citations, and sample plots for two alternative methods are provided as Fig. S5 and S6 in the ESI.†

The methylene bead mobility was evaluated by monitoring the evolution of mean-squared displacement (MSD) of all beads that comprise an SCPN with time. The MSD of methylene beads were recorded over 1 ns from an already equilibrated particle state.

All quantities were calculated as averages of 3 distinct particles each equilibrated over 10 different times in order to obtain trends independent of the exact SCPN configuration. Reference sizes were taken over all 3 particles and an extended equilibration period. These reference sizes were used for setting the initial plate distance and choosing the area for stress calculations.

3 Results and discussion

3.1 Initial structure

A typical SCPN at 300 K is shown in Fig. 3, this 1000 monomer particle has been functionalized with 10% cross-linking. At any snapshot in time the particle is roughly spheroidal with an average radius of 23 Å and typical deviation of any axis of 7% of the average radius. Locations of each methylene bead within a particle fluctuate significantly with a standard deviation of the particle semi-major axis of 0.3 Å over time. The average size of the particle can be readily visualized through the radial density distribution (Fig. 4). The collapsed linear chain has roughly uniform density throughout and drops rapidly as the edge of the particle is reached. This density matches that of bulk PE previously simulated using the same force field.[35] Since all collapsed linear chains have this density, particles with a greater DP are larger. Interestingly, particle size is nearly independent of the degree of cross-linking with only a slight reduction in the drop-off radius as the degree of cross-linking is increased up to 15%. This implies that the addition of cross-links to the SCPN does not change the equilibrium dimension of the SCPN in vacuum, this does not however imply that the size is independent of the degree of cross-linking in the presence of solvents or neighboring polymers. The particle size is weakly temperature dependent with radius increasing by 11% from 300 K to 500 K for the linear particle and by 3% for the 10% cross-linked SCPN.

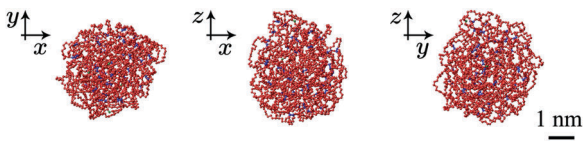

Fig. 3 Snapshots of a 1000 monomer 10% cross-link SCPN from three orthogonal views.

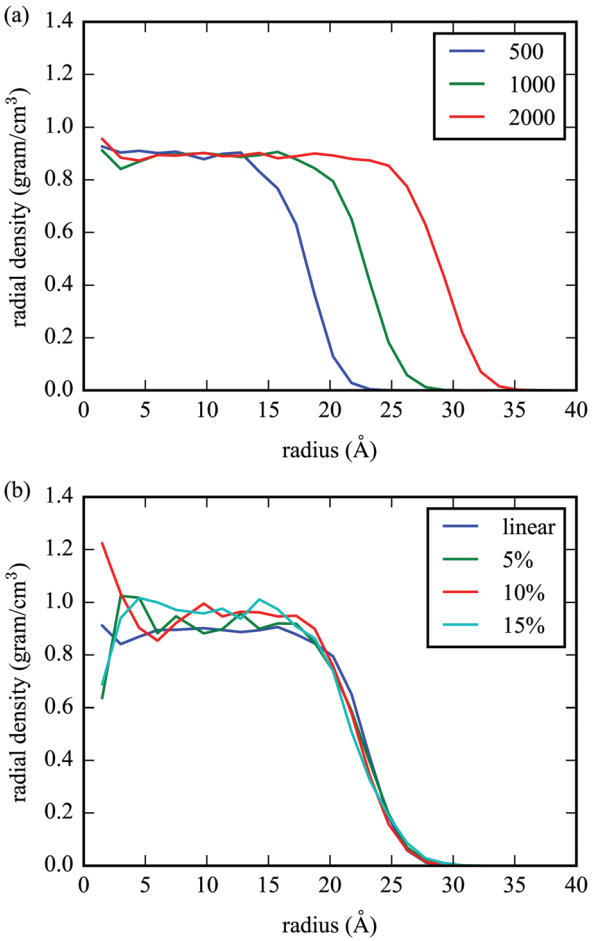

Fig. 4 Radial density distribution of equilibrated (a) collapsed linear chains as a function of number of monomers, (b) 1000 monomer long chain and SCPNs as a function of degree of cross-linking.

The glass transition temperature of the various SCPNs is measured by cooling the particles at a constant rate from 500 K down to 10 K while monitoring the total energy. For all particles a distinct change in the slope of the total energy *versus* temperature curve is observed. This typical response is shown for the specific case of the 1000 monomer long particle with 10% cross-linking, which was found to have a transition temperature of 253.23 K (Fig. 5a). The transition was found to be rate dependent with the change obscured at rates that are too high as detailed in Fig. S4 in the ESI.† This T_g is lower than that of bulk PE simulated with the same forcefield,[35] this suppression is expected for a small isolated particle.[51] While there are no statistically significant trends in the glass transition temperature with either the DP or the percent cross-linking, there does seem to be an increase in T_g with increasing percent cross-linking (Fig. 5b). Critically, from these particle cooling simulations we identified 300 K as rubbery and 150 K as glassy for all particles. We will use these two temperatures to examine the differences in behavior of SCPN in the glassy and rubbery states.

The potential energy of the equilibrated SCPN depends on both the number of monomers and the degree of cross-linking as shown in Fig. 6. The potential energy in a collapsed linear

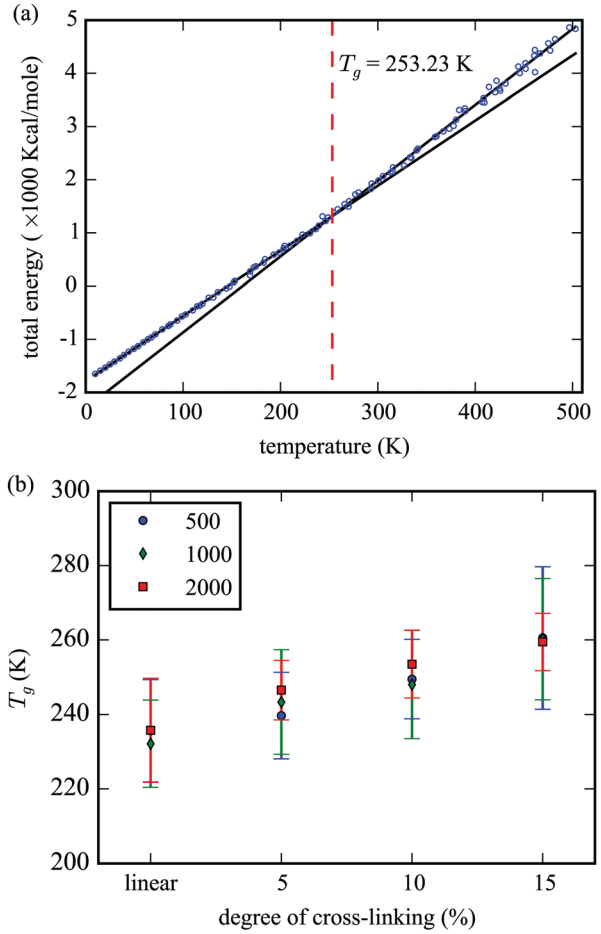

Fig. 5 Glass transition temperature dependence of SCPN structure. (a) Total energy change of 1000 monomer 10% cross-link SCPN with cooling from processing temperature of 500 K. (b) Transition temperature as a function of degree of cross-linking. Standard deviation shown for 30 different configurations for each case.

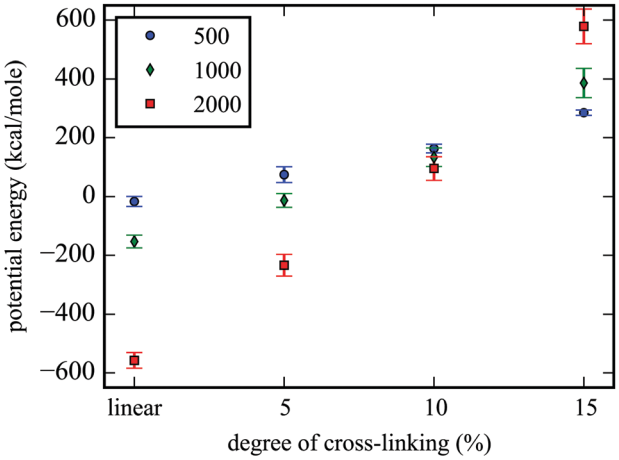

Fig. 6 Total potential energy *versus* degree of cross-linking for each degree of polymerization. Standard deviation shown for 30 different configurations for each case.

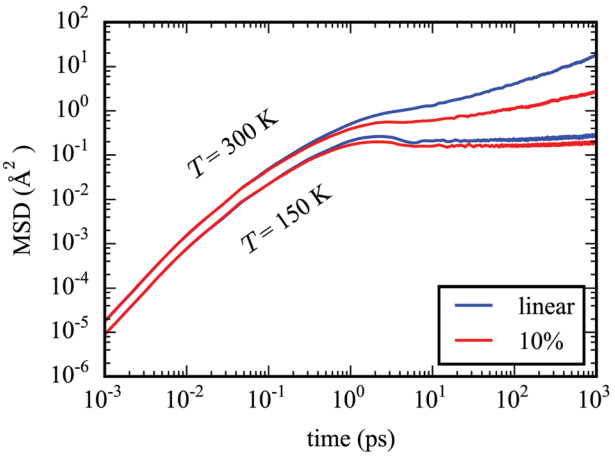

Fig. 7 Logarithmic plot of the MSD *versus* time of 1000 monomer linear collapsed chain and 10% cross-link SCPN at 300 K and 150 K.

chain (no cross-linking) scales down linearly with the increasing DP since at near equilibrium spacing the non-bonded energy among monomers is negative. As cross-links are added to the collapsed linear chain, the potential energy increases with the increasing degree of cross-linking. The new bond lengths, angles, and dihedrals have equivalent distribution about equilibrium as the original bond lengths, angles, and dihedrals (ESI,† Fig. S2). The change in energy with increasing degree of cross-linking within each SCPN is roughly equal to the sum of the energies added by each new bond, angle, and dihedral. There is minimal associated non-bonded energy change because the radial density does not change. As cross-links are added, the potential energy for SCPN with more monomers increases more than the energy for that with fewer monomers, primarily due to the greater quantity of monomers and cross-links present.

We calculated the methylene bead MSD at both 300 K and 150 K (Fig. 7 and Table 2) in order to understand chain mobility for potential interaction within a bulk polymer formed from assemblies of SCPN. All particles exhibit first a ballistic regime ($\propto t^2$) and then a sub diffusive regime. At 150 K the post-ballistic slope is near zero, whereas at 300 K it is 0.635 and 0.378 for 1000 monomer linear collapsed chain and 10% crosslink SCPN, respectively. This temperature dependence is consistent with our expectation from the T_g studies that indicated that the 150 K particles would behave in a glassy manner whereas the 300 K particles would behave in a rubbery manner. The addition of cross-links to the collapsed linear chain monotonically decreases

Table 2 Slope of mean square displacement *versus* time on a log–log plot at 1 ns of methylenes that compose SCPNs as a function of degree of cross-linking and degree of polymerization [Å^2 ps^{-1}]

		Linear	5%	10%	15%
300 K	500	0.578	0.494	0.376	0.288
	1000	0.635	0.472	0.378	0.285
	2000	0.582	0.477	0.338	0.278
150 K	500	0.142	0.097	0.106	0.074
	1000	0.096	0.138	0.071	0.049
	2000	0.117	0.106	0.069	0.049

the mobility. At 300 K this reduction in mobility is pronounced with a factor of 10 reduction from the collapsed linear chain to SCPN with 15% of degree of cross-linking at 1 ns. At 150 K the effect of cross-linking is muted compared to the influence of cross-linking at 300 K with only a factor of 2 reduction from the collapsed linear chain to SCPN with 15% of degree of cross-linking.

3.2 Response to compression

When an SCPN is subjected to monotonic compressive loading by rigid flat plates, the particle accommodates the imposed boundary condition through shape change (Fig. 8). Initially the particle becomes nominally cylindrical and then continues to grow in radius as the height decreases. The stress increases monotonically with increasing strain in a concave up manner (Fig. 9a). This overall stress response has two distinct origins: the shape change effect (low initial contact area between plate and spheroidal SCPN) and the intrinsic material/atomistic response. We can further examine the intrinsic material response by examining how the energy changes under compression (Fig. 9b).

The total potential energy increases monotonically with a concave up shape as the particle is compressed. Breaking the potential energy down into specific interaction potentials elucidates how the SCPN accommodates the applied deformation. Each individual interaction potential increases with the same shape as the overall potential energy. The smallest contributor to the change in potential energy is the bond stretching energy, which does have some fluctuation but is effectively unchanged throughout the simulation. The bond angle energy has a greater contribution than the bond stretching energy, but still only around 15% of total change in potential energy. The largest of the bonded interactions is the torsional dihedral, which accounts for around 1/3 of the total energy change. Non-bonded energy accounts for half of total change in potential energy indicating that the relative bead displacements from disparate parts of the chain govern the stress response. This large contribution of non-bonded energy under mechanical loading is typical for polymers above T_g.[35,52–55] The bond-stretching, angle bending, and torsional dihedral interactions associated with the cross-links have equivalent change in energy as their respective contributions from the initial linear structure. This equivalence implies that while the cross-links may influence how the particle deforms, once they are formed they are energetically indistinguishable from the rest of the SCPN (Fig. S15, ESI†).

The stress response of the SCPN as a function of percent cross-linking and DP at 300 K is shown in Fig. 9. The stress-response of

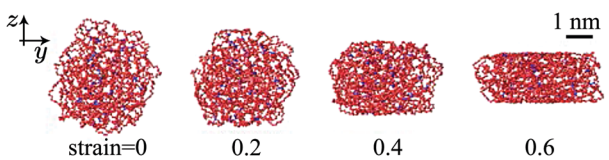

Fig. 8 Snapshots of a MD simulation of 1000 monomer 10% cross-link SCPN under compression at 300 K. Red beads are standard monomers and blue beads are cross-linked monomers (Fig. S8, ESI†).

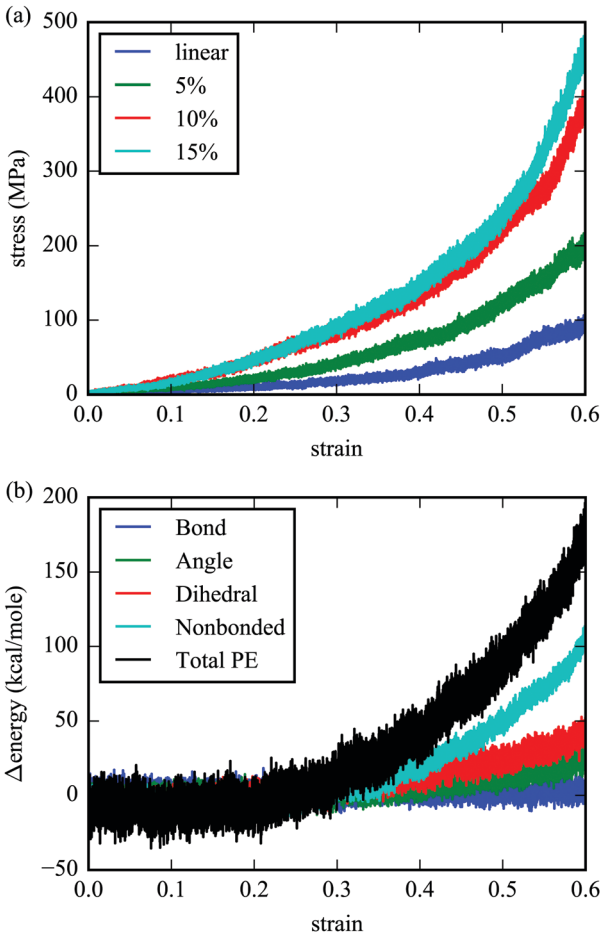

Fig. 9 Compression response of 1000 monomer SCPN at 300 K. (a) Stress *versus* strain as a function of degree of cross-linking. (b) Potential energy components for 10% cross-link SCPN.

the SCPN can be tailored by modifying the degree of cross-linking. The higher the degree of cross-linking, the stiffer the response and the more hyperelastic the response over the simulated range. The cross-links reduce relative atom motion by increasing connectivity within the chain. Fig. 10 shows the stress for each SCPN type at a strain of 0.3. While the degree of cross-linking dependence is apparent despite the large standard deviation, the stress response shows negligible dependence on DP within the simulated range of 500 to 2000 monomers. Naturally, the force response does change with number of monomers since larger particles have larger initial cross-sectional area. For all degrees of cross-linking and polymerization the stress response is qualitatively similar at 300 K (ESI,† Fig. S9–S12).

The SCPNs below the glass transition temperature behave both quantitatively and qualitatively different than above T_g (Fig. 11). In contrast to the 300 K response, the typical 150 K stress response has three apparent regions: an increasing region followed by a relatively flat portion, and then a second increasing region at a higher slope than the first. This behavior resembles that of a foam with the stress growing rapidly after the structure has compacted. In contrast to at 300 K the initial stiffness does not appear to depend on degree of cross-linking,

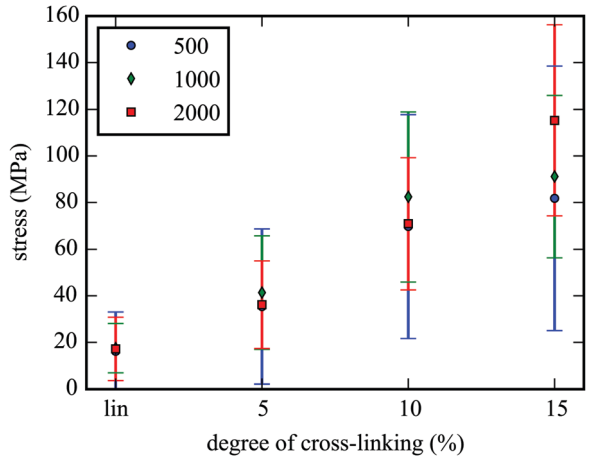

Fig. 10 Stress response of SCPN at 300 K at a strain of 0.3 as a function of degree of cross-linking and degree of polymerization. Standard deviation shown for 30 different configurations for each case.

however the stress values among the different cross-linking degrees deviate further at larger strains with larger stresses for higher degree of cross-linking. This deviation comes in part from the higher plateau stress and in part from the decreased length of the plateau region for higher degree of cross-linking compared to lower degree of cross-linking. Overall, the stress and potential energy associated with compression at 150 K are significantly higher than at 300 K as would be expected for a glassy *versus* rubbery response for the same material. At 150 K the dihedral energy is comparable to the non-bonded energy with each accounting for nearly half of the total potential energy, and the remaining energy arising from angle deformation. While non-bonded, dihedral, and angle energies are all increased relative to the 300 K case, the relative importance of the covalent interactions to non-covalent interactions is greater at 150 K. Further, the ratio of dihedral energy to non-bonded energy increases with increasing degree of cross-linking (Fig. S14, ESI†). The increased prevalence of bonded interactions relative to non-bonded has been seen in bulk cross-linked glassy polymers as well.[55] The similar dependence of the mechanical behavior of SCPN and bulk polymers on temperature relative to T_g and degree of cross-linking suggests that we should be able to apply knowledge gained from decades of bulk polymer research to tailoring SCPN mechanical response.

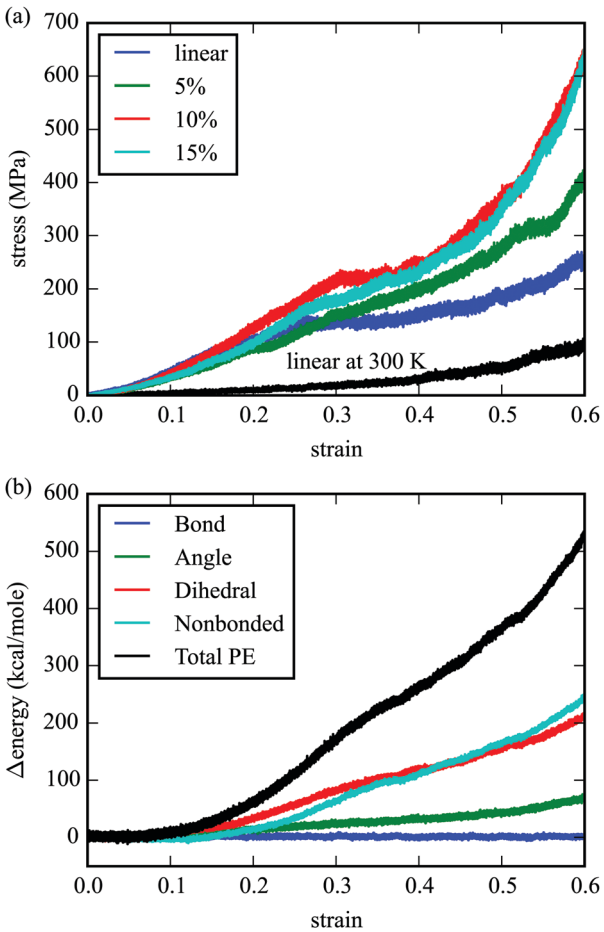

Fig. 11 Compression response of 1000 monomer SCPN at 150 K. (a) Stress *versus* strain as a function of degree of cross-linking. (b) Potential energy components for 10% cross-link SCPN.

4 Conclusions

In this study we created MD models of polyethylene-like SCPNs and used them to investigate the thermo-mechanical properties of SCPNs as a function of degree of cross-linking and DP. In particular, three different numbers of monomers (500, 1000, 2000) and four different degrees of cross-linking (collapsed linear, 5%, 10%, 15%) were investigated. The molecular structure was coarse-grained into beads consisting of a single methylene group with interactions described by the modified Dreiding potential. These particles were analyzed in terms of glass transition temperature, bead mobility, potential energy, and stress response to flat plate compression. 150 K and 300 K were used as the representative temperatures for glassy and rubbery behavior respectively.

We observed that SCPN mechanical properties can be modified by changing internal ratio of cross-linking but not DP, conversely SCPN size can be modified by DP but not by ratio of cross-linking, although there is minimal difference between 10% and 15%. At 300 K the SCPNs follow a typical non-linear rubbery behavior with higher degree of cross-linking corresponding to higher stress throughout the applied deformation. At 150 K the SCPNs show three distinct regions, the slope of the initial region is independent of degree of cross-linking, the subsequent plateau and second increasing region have stress that does scale with the degree of cross-linking. The associated potential energy is also temperature dependent both in terms of overall magnitude and relative values of the underlying components. At both temperatures non-bonded energy is the largest contribution to the overall increase in potential energy with compression. The relative contribution of the dihedral torsional energy increases with both increasing degree of cross-linking and decreasing temperature such that at 15% and 150 K

the dihedral energy is comparable to the non-bonded energy. In all cases bond and angle distortion is relatively minor. These results suggest that mechanical property tailoring of an individual SCPN should only weakly depend on the stiffness of the cross-link since the cross-link mostly acts by the locking the structure into a particular relative configuration. Consequently, the cross-links have greater effect above T_g and at large deformation below T_g than they do for small deformation below T_g where even the linear structure has minimal mobility.

The mobility of methylenes that compose the SCPN has important implications for how the SCPN will interact in bulk assemblies. The slope of mobility on a log–log plot of methylenes within the collapsed linear chain at 300 K is halved with the addition of 15% cross-linking. This mobility is still significantly larger than the motion of methylenes below T_g suggesting a potential for creating entanglements among beads through SCPN assembly processing above T_g. Given the reduced mobility of methylenes with increasing degree of cross-linking at both temperatures we expect less ductile bulk assembly behavior with increasing degree of intramolecular cross-linking. The contrast between behavior at 150 K and 300 K should however be much larger than the cross-link dependence at either temperature given the drastic difference in both the individual particle mechanical properties and the expected inter-particle interaction. Work is underway to experimentally validate these predicted trends for both the single particle and bulk assembly mechanical behavior.

Acknowledgements

This material is based on work which used the Extreme Science and Engineering Discovery Environment (XSEDE),[56] which is supported by National Science Foundation grant number ACI-1053575, and is supported by the Israel Science Foundation under grant number 920/15.

References

1 K. Min, M. Silberstein and N. R. Aluru, *J. Polym. Sci., Part B: Polym. Phys.*, 2014, **52**, 444–449.
2 J. R. Galli and P. Gibbs, *Acta Metall.*, 1964, **12**, 775–778.
3 C. Li and A. Strachan, *Polymer*, 2010, **51**, 6058–6070.
4 A. Bandyopadhyay, P. K. Valavala, T. C. Clancy, K. E. Wise and G. M. Odegard, *Polymer*, 2011, **52**, 2445–2452.
5 J.-Y. Sun, X. Zhao, W. R. K. Illeperuma, O. Chaudhuri, K. H. Oh, D. J. Mooney, J. J. Vlassak and Z. Suo, *Nature*, 2012, **489**, 133–136.
6 J. Zhao, P. Yu and S. Dong, *Materials*, 2016, **9**, 234.
7 J. Y. He, Z. L. Zhang, H. Kristiansen, K. Redford, G. Fonnum and G. I. Modahl, *eXPRESS Polym. Lett.*, 2013, **7**, 365–374.
8 E. F. Cluff, E. K. Gladding and R. Pariser, *J. Polym. Sci.*, 1960, **45**, 341–345.
9 P. J. Flory, N. Rabjohn and M. C. Shaffer, *J. Polym. Sci.*, 1949, **4**, 435–455.
10 N. D. G. Zhixin Wang and Alex A. Volinsky, *J. Appl. Polym. Sci.*, 2014, **131**, 41050.
11 X. Zhu, Y. Zhou and D. Yan, *J. Polym. Sci., Part B: Polym. Phys.*, 2011, **49**, 1277–1286.
12 J. M. Frechet, *Science*, 1994, **263**, 1710–1715.
13 M. L. Gardel, J. H. Shin, F. C. MacKintosh, L. Mahadevan, P. Matsudaira and D. A. Weitz, *Science*, 2004, **304**, 1301–1305.
14 S. J. Garcia, *Eur. Polym. J.*, 2014, **53**, 118–125.
15 A. M. Hanlon, C. K. Lyon and E. B. Berda, *Macromolecules*, 2016, **49**, 2–14.
16 A. E. Cherian, F. C. Sun, S. S. Sheiko and G. W. Coates, *J. Am. Chem. Soc.*, 2007, **129**, 11350–11351.
17 M. Ouchi, N. Badi, J.-F. J. Lutz and M. Sawamoto, *Nat. Chem.*, 2011, **3**, 917–924.
18 A. Sanchez-Sanchez, S. Akbari, A. Etxeberria, A. Arbe, U. Gasser, A. J. Moreno, J. Colmenero and J. A. Pomposo, *ACS Macro Lett.*, 2013, **2**, 491–495.
19 S. Mavila, C. E. Diesendruck, S. Linde, L. Amir, R. Shikler and N. G. Lemcoff, *Angew. Chem., Int. Ed.*, 2013, **52**, 5767–5770.
20 J. A. Kaitz, C. M. Possanza, Y. Song, C. E. Diesendruck, A. J. H. Spiering, E. W. Meijer and J. S. Moore, *Polym. Chem.*, 2014, **5**, 3788.
21 S. Mavila, O. Eivgi, I. Berkovich and N. G. Lemcoff, *Chem. Rev.*, 2016, **116**, 878–961.
22 J.-F. Lutz, J.-M. Lehn, E. W. Meijer and K. Matyjaszewski, *Nat. Rev. Mater.*, 2016, **1**, 16024–16037.
23 K. Watanabe, R. Tanaka, K. Takada, M.-J. Kim, J.-S. Lee, K. Tajima, T. Isono and T. Satoh, *Polym. Chem.*, 2016, **7**, 4782–4792.
24 P. Frank, A. Prasher, B. Tuten, D. Chao and E. Berda, *Appl. Petrochem. Res.*, 2015, **5**, 9–17.
25 N. Hosono, A. M. Kushner, J. Chung, A. R. A. Palmans, Z. Guan and E. W. Meijer, *J. Am. Chem. Soc.*, 2015, **137**, 6880–6888.
26 J. He, L. Tremblay, S. Lacelle and Y. Zhao, *Soft Matter*, 2011, **7**, 2380.
27 F. M. Capaldi, M. C. Boyce and G. C. Rutledge, *Polymer*, 2004, **45**, 1391–1399.
28 E. Jaramillo, N. Wilson, S. Christensen, J. Gosse and A. Strachan, *Phys. Rev. B: Condens. Matter Mater. Phys.*, 2012, **85**, 024114.
29 R. S. Hoy and M. O. Robbins, *J. Polym. Sci., Part B: Polym. Phys.*, 2006, **44**, 3487–3500.
30 A. V. Lyulin, N. K. Balabaev, M. A. Mazo and M. A. J. Michels, *Macromolecules*, 2004, **37**, 8785–8793.
31 J. Han, R. H. Gee and R. H. Boyd, *Macromolecules*, 1994, **27**, 7781–7784.
32 F. Müller-Plathe, *ChemPhysChem*, 2002, **3**, 754–769.
33 S. J. V. Frankland, A. Caglar, D. W. Brenner and M. Griebel, *J. Phys. Chem. B*, 2002, **106**, 3046–3048.
34 G. M. Odegard, T. C. Clancy and T. S. Gates, *46th AIAA/ASME/ASCE/AHS/ASC structures, structural dynamics, and materials conference*, Austin, TX, 2005, pp. 18–21.
35 D. Hossain, M. Tschopp, D. Ward, J. Bouvard, P. Wang and M. Horstemeyer, *Polymer*, 2010, **51**, 6071–6083.
36 S. L. Mayo, B. D. Olafson and W. A. Goddard, *J. Phys. Chem.*, 1990, **94**, 8897–8909.
37 B. R. Brooks, R. E. Bruccoleri, B. D. Olafson, D. J. States, S. Swaminathan and M. Karplus, *J. Comput. Chem.*, 1983, **4**, 187–217.

38 H. J. C. Berendsen, D. van der Spoel and R. van Drunen, *Comput. Phys. Commun.*, 1995, **91**, 43–56.
39 *Physical Properties of Polymers Handbook*, ed. J. E. Mark, Springer Science & Business Media, LLC, New York, 2nd edn, 2007.
40 J. Zhao, S. Nagao, G. M. Odegard, Z. Zhang, H. Kristiansen and J. He, *Nanoscale Res. Lett.*, 2013, **8**, 541.
41 J. Wu, J. He, G. M. Odegard and Z. Zhang, *Nanoscale Res. Lett.*, 2013, **8**, 322.
42 P. Valentini, W. W. Gerberich and T. Dumitrică, *Phys. Rev. Lett.*, 2007, **99**, 175701.
43 A. J. Moreno, F. Lo Verso, A. Sanchez-Sanchez, A. Arbe, J. Colmenero and J. A. Pomposo, *Macromolecules*, 2013, **46**, 9748–9759.
44 F. Lo Verso, J. A. Pomposo, J. Colmenero and A. J. Moreno, *Soft Matter*, 2015, **11**, 1369–1375.
45 S. Plimpton, *J. Comput. Phys.*, 1995, **117**, 1–19.
46 K. Fukui, B. G. Sumpter, M. D. Barnes and D. W. Noid, *Macromolecules*, 2000, **33**, 5982–5987.
47 L.-h. Tam and D. Lau, *RSC Adv.*, 2014, **4**, 33074.
48 V. Varshney, S. S. Patnaik, A. K. Roy and B. L. Farmer, *Macromolecules*, 2008, **41**, 6837–6842.
49 K. Fukui, B. Sumpter, M. Barnes and D. Noid, *Comput. Theor. Polym. Sci.*, 1999, **9**, 245–254.
50 K. Fukui, B. G. Sumpter, M. D. Barnes and D. W. Noid, *Polym. J.*, 1999, **31**, 664–671.
51 W. L. Merling, J. B. Mileski, J. F. Douglas and D. S. Simmons, *Macromolecules*, 2016, **49**, 7597–7604.
52 S. Soon Jang and W. H. Jo, *Polymer*, 1999, **40**, 919–925.
53 A. A. Pacheco and R. C. Batra, *Polymer*, 2013, **54**, 819–840.
54 N. Vu-Bac, M. A. Bessa, T. Rabczuk and W. K. Liu, *Macromolecules*, 2015, **48**, 6713–6723.
55 J. C. Moller, G. S. Kedziora, S. A. Barr, T. D. Breitzman and R. J. Berry, *Comput. Mater. Sci.*, 2017, **128**, 257–277.
56 J. Towns, T. Cockerill, M. Dahan, I. Foster, K. Gaither, A. Grimshaw, V. Hazlewood, S. Lathrop, D. Lifka, G. D. Peterson, R. Roskies, J. R. Scott and N. Wilkins-Diehr, *Comput. Sci. Eng.*, 2014, **16**, 62–74.

